

# SYMMETRIC LOCAL ABSORBING BOUNDARIES IN TIME AND SPACE

By Loukas F. Kallivokas,<sup>1</sup> Associate Member, ASCE, Jacobo Bielak,<sup>2</sup>  
Member, ASCE, and Richard C. MacCamy<sup>3</sup>

**ABSTRACT:** This paper is concerned with the development of simple, yet accurate, absorbing boundaries that can be incorporated readily into existing finite element programs directly in the time domain. The wave equation in a two-dimensional exterior domain is considered as a prototype situation. For this problem a family of approximate absorbing boundary elements is constructed by an asymptotic expansion procedure. Each element is completely determined by a pair of local, symmetric, stiffnesslike and dampinglike constant matrices, coupled only through adjoining nodes. This makes it possible to combine the new boundary elements with standard finite elements used to represent the interior domain via ordinary assembly procedures, while preserving the symmetry and bandwidth of the global matrices. Results of numerical experiments for a circular geometry confirm that accuracy increases with the order of the approximations, with the radius of the absorbing boundary, and with the dominant frequencies of the excitation. This implies that the higher the frequency of the excitation the smaller the size of the buffer annulus required to attain a desired accuracy.

## INTRODUCTION

There is a wide range of engineering problems that require solving time-dependent equations in infinite or semi-infinite regions. Explicit solutions to problems in infinite domains are possible only in certain cases that involve simple geometries and linear, homogeneous materials, while for general situations one must resort to numerical methods. One common approach for solving wavelike equations involving exterior regions is via integral representations, a method well suited for frequency domain formulations of time-harmonic linear problems. An alternative technique for the numerical approximation of solutions directly in the time domain involves the reduction of the infinite medium to a finite region by introducing an artificial boundary on which one must specify some condition to prevent spurious wave reflections. There will be a theoretical exact condition tantamount to an integral equation formulation, but this will be nonlocal in both time and space and difficult to determine. Thus, there has been extensive work on devising approximate conditions that are more localized in time, space, or both. Among the many references on this subject one notes for example Lysmer and Kuhlemeyer (1969), Engquist and Majda (1977, 1979), Kriegsmann and Morawetz (1978), Bayliss and Turkel (1980), Geers and Felippa (1983), and Kriegsmann et al. (1987). Surveys include Robinson (1977), Kausel and Tassoulas (1981), Cohen and Jennings (1983), and Kausel (1988), while assessments of the numerical performance of various methods are given by Wolf (1986), Blaschak and Kriegsmann (1988), and Halpern and Trefethen (1988).

---

<sup>1</sup>Swanson Analysis Systems Grad. Fellow, Dept. of Civ. Engrg., Carnegie Mellon Univ., Pittsburgh, PA 15213.

<sup>2</sup>Prof., Dept. of Civ. Engrg., Carnegie Mellon Univ., Pittsburgh, PA.

<sup>3</sup>Prof., Dept. of Mathematics, Carnegie Mellon Univ., Pittsburgh, PA.

Note. Discussion open until February 1, 1992. To extend the closing date one month, a written request must be filed with the ASCE Manager of Journals. The manuscript for this paper was submitted for review and possible publication on September 6, 1990. This paper is part of the *Journal of Engineering Mechanics*, Vol. 117, No. 9, September, 1991. ©ASCE, ISSN 0733-9399/91/0009-2027/\$1.00 + \$.15 per page. Paper No. 26149.

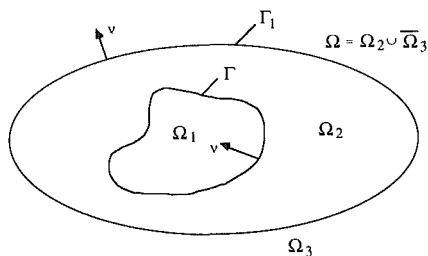


**FIG. 1. Cavity Subjected to Antiplane Shear Traction on  $\Gamma$ ;  $\Gamma_1 =$  Artificial Boundary**

A prototype of the situation just mentioned is the solution of the wave equation in an exterior domain. This has been a typical model problem in the aforementioned references and will be here also. Specifically, let  $\Gamma$  be a closed curve in the plane with exterior  $\Omega$  and interior  $\Omega_1$ . Let  $\mathbf{x}$  denote position and  $t$  time. We seek  $u(\mathbf{x}, t)$  such that:

$$\Delta u = \frac{1}{\beta^2} u_{tt}, \quad \mathbf{x} \in \Omega, \quad t > 0 \dots\dots\dots (1a)$$

$$\mu u_\nu = \tau_0 p \text{ on } \Gamma, \quad t > 0 \dots\dots\dots (1b)$$

$$u(\mathbf{x}, 0) = 0 = u_t(\mathbf{x}, 0) \text{ in } \Omega \dots\dots\dots (1c)$$

In addition,  $u(\mathbf{x}, t)$  is required to be outgoing;  $\beta$ ,  $\mu$ , and  $\tau_0$  = prescribed constants;  $p$  = a prescribed (dimensionless) function of position and time;  $\Delta$  = the Laplacian operator,  $\nu$  = the outgoing unit normal to  $\Gamma$  and subscripts following the state variable denote partial derivatives. Physically (1a)–(1c) may be given several different interpretations (acoustics, electromagnetism, etc.), but to fix ideas we will regard  $u$  as the displacement field in the closure  $\bar{\Omega} = R^2 \setminus \Omega_1$  of  $\Omega$  produced by an antiplane shear traction  $\tau = \tau_0 p(\mathbf{x}, t)$  applied on the boundary  $\Gamma$  of the cavity  $\Omega_1$ . The exterior domain  $\Omega$  is occupied by an elastic, homogeneous material, initially at rest, with shear modulus  $\mu$  and mass density  $\rho$ ;  $\beta = \sqrt{\mu/\rho}$  is then the velocity of shear (SH) wave propagation. The traction  $\tau$  is related to the displacement  $u$  through the constitutive law:

$$\tau = \mu u_\nu \dots\dots\dots (2)$$

We follow the usual procedure of introducing an artificial boundary  $\Gamma_1$  in  $\Omega$  (Fig. 1) and obtaining an approximate condition on  $\Gamma_1$ . Using the ideas of Barry et al. (1988) this produces an approximate condition that contains an arbitrary parameter  $\delta$ . Our paper has two main goals:

1. To implement the approximate problem over the truncated region, for any  $\delta$ , by variational finite element methods. This is in contrast to the usual finite difference procedures. Two approaches are considered for the numerical implementation. One is a mixed method that introduces the traction on the absorbing boundary as an independent state variable. The other is in the same vein as the well-known viscous damper approach (Lysmer and Kuhlemeyer 1969); specifically, it is shown that the spatially discretized versions of the approximate local boundary conditions can be cast in terms of symmetric time-invariant stiffness-like and dampinglike matrices that can be incorporated directly into the standard

finite element equations of motion for the interior domain. This implementation is quite natural and can be achieved by using standard finite element software for *interior* elasticity problems.

2. To present the results of a series of numerical experiments on the special case of circular geometry so that one can study errors. An analysis of these errors confirms the effectiveness of the variational technique. The effect of tuning the parameter  $\delta$  is also explored. We indicate the effect of changing the position of the artificial boundary and the frequency spectrum of the input data  $p$  in (1b). The effect of the absorbing boundary on the response of various angular modes is also determined.

### MATHEMATICAL ANALYSIS

Suppose  $\Gamma_1$  is a closed, convex and smooth curve containing  $\Omega_1$  in its interior. Then on  $\Gamma_1$   $u$  will satisfy a nonlocal condition for the traction  $\tau$  of the form:

$$\tau(\mathbf{x}, t) = \mu u_{\nu}(\mathbf{x}, t) = \int_0^t \int_{\Gamma_1} K(|\mathbf{x} - \boldsymbol{\xi}|, t - \zeta) u(\boldsymbol{\xi}, \zeta) d\boldsymbol{\xi} d\zeta, \quad \mathbf{x} \in \Gamma_1, \quad t > 0 \dots \dots \dots (3)$$

where  $\nu$  here is the outer normal to  $\Gamma_1$ . The right-hand side denotes an operator that involves the values of  $u(\boldsymbol{\xi}, \zeta)$  for  $\boldsymbol{\xi}$  ranging over  $\Gamma_1$  and  $\zeta$  from 0 to  $t$ . The kernel  $K$  depends both on position and time. Eq. (3) may be written symbolically as:

$$\tau(\mathbf{x}, t) = \mu u_{\nu}(\mathbf{x}, t) = \mathcal{F}[u^t(\cdot, \cdot)](\mathbf{x}), \quad \mathbf{x} \in \Gamma_1, \quad t > 0 \dots \dots \dots (4)$$

in which  $\mathcal{F}$  = the exact operator expressing the spatial and temporal nonlocality on  $\Gamma_1$ . The superscript  $t$  over  $u$  on the right-hand side of (4) indicates that  $\mathcal{F}$  depends on the entire history of  $u$  up to time  $t$ . In other words,  $\mathcal{F}$  merely expresses the fact that the motion at every point on the artificial boundary  $\Gamma_1$  is coupled with the time histories of all other points on  $\Gamma_1$ . Theoretically, one could obtain  $\mathcal{F}$  by solving (1a) in the exterior region  $\Omega_3$  (Fig. 1) for given values  $u|_{\Gamma_1}$  on  $\Gamma_1$  and then computing the normal derivative on  $\Gamma_1$ .

The immediate objective now is to approximate  $\mathcal{F}$  so as to reduce the temporal nonlocality. The strategy is to recast the problem in the Laplace transform domain and to seek asymptotic expansions that are outgoing and valid for large values of the transform variable. It turns out that this procedure also automatically reduces the spatial nonlocality on  $\Gamma_1$ . Herein we give only the basic outline. Details can be found in Barry et al. (1988) and Kallivokas (1990).

One studies the following problem in the region  $\Omega_3$  exterior to  $\Gamma_1$  (Fig. 1):

$$\Delta \hat{V} = \frac{s^2}{\beta^2} \hat{V} \text{ in } \Omega_3 \dots \dots \dots (5a)$$

$$\hat{V}(\mathbf{x}, s; t) = u(\mathbf{x}, t) \text{ on } \Gamma_1 \dots \dots \dots (5b)$$

in which  $s$  = the Laplace transform variable. In addition to satisfying (5a) and (5b),  $\hat{V}$  is required to be an outgoing solution. (To say that  $\hat{V}$  is outgoing means that if  $Res > 0$ , then  $\hat{V}$  should tend to zero as  $|\mathbf{x}|$  tends to infinity. In the time domain this will simply mean that, for a fixed value of  $t$ , the

solution would be identically zero when  $|\mathbf{x}|$  is large enough.) Since (5a) is identical to the transformed version of (1a), and  $\hat{V}$  is outgoing and coincides with  $u$  on  $\Gamma_1$  by (5b), it follows that the Laplace transform  $\hat{u}$  of the exact solution  $u$  of (1a)–(1c) must coincide over  $\Omega_3$  with the Laplace transform of  $\hat{V}$ . Then, one may use  $\hat{V}$  instead of  $\hat{u}$  in order to obtain an approximation for the absorbing operator  $\mathcal{F}$  in (4). Borrowing from geometrical optics (Whitham 1974), consider a high-frequency expansion for  $\hat{V}$  of the following form:

$$\hat{V}(\mathbf{x}, s; t) \sim e^{-s\phi(\mathbf{x})} \sum_{k=0}^{\infty} s^{-k} V^k(\mathbf{x}; t) \text{ in } \Omega_3 \dots\dots\dots (6a)$$

subject to the constraints:

$$\phi(\mathbf{x}) = 0; \quad V^0(\mathbf{x}; t) = u(\mathbf{x}, t); \quad V^k(\mathbf{x}; t) = 0, \quad k \geq 1, \text{ on } \Gamma_1 \dots\dots (6b)$$

Eqs. (6a) and (6b) ensure that  $\hat{V}$  is outgoing and that (5b) is satisfied for arbitrary functions  $\phi$  and  $V^k$ ,  $k \geq 1$ . By introducing (6a) and (6b) into (5a), and matching the coefficients of the various powers of  $s$ , one obtains a set of recursive differential equations involving the unknown functions  $\phi$  and  $V^k$ . In order to approximate  $\mathcal{F}$  on  $\Gamma_1$ , it is necessary to determine  $V^k$  and its derivatives only on  $\Gamma_1$  rather than throughout the entire region  $\Omega_3$ . This may be done directly from the recursive equations without solving explicitly for  $\hat{V}$  throughout  $\Omega_3$ . One can, thus, obtain expansions for  $\hat{V}$  and  $\hat{V}_v$  on  $\Gamma_1$  in terms of the functions  $V^k$  and their derivatives, evaluated on  $\Gamma_1$ . This process leads to an expression for the Laplace transform of the traction  $\tau$  of the form:

$$\hat{\tau} = \mu \hat{u}_v(\mathbf{x}, s) = \sum_{m=-1}^{\infty} \Phi_m[\hat{u}(\cdot, s)](\mathbf{x}) s^{-m} \dots\dots\dots (7)$$

in which  $\Phi_m$  are known spatial differential operators acting on  $\hat{u}$ . Then from (4) and (7) one obtains the desired expression for the Laplace transform of  $\mathcal{F}$ :

$$\hat{\mathcal{F}}[s, \hat{u}(\cdot, s)](\mathbf{x}) = \sum_{m=-1}^{\infty} \Phi_m[\hat{u}(\cdot, s)](\mathbf{x}) s^{-m} \dots\dots\dots (8)$$

The first three  $\Phi_m$ 's are given as:

$$\Phi_{-1}[\hat{u}(\mathbf{x}, s)] = -\frac{\mu}{\beta} \hat{u}(\mathbf{x}, s) \dots\dots\dots (9a)$$

$$\Phi_0[\hat{u}(\mathbf{x}, s)] = \frac{\mu}{2} \kappa(\mathbf{x}) \hat{u}(\mathbf{x}, s) \dots\dots\dots (9b)$$

$$\Phi_1[\hat{u}(\mathbf{x}, s)] = \frac{\beta\mu}{2} \hat{u}_{\lambda\lambda}(\mathbf{x}, s) + \frac{\beta\mu}{8} \kappa(\mathbf{x})^2 \hat{u}(\mathbf{x}, s) \dots\dots\dots (9c)$$

where  $\kappa(\mathbf{x})$  = the curvature of  $\Gamma_1$  at  $\mathbf{x}$  and the subscripts  $\lambda$  denote tangential derivatives. We adopt the convention that the curvature is negative. Thus for a circle of radius  $R$ ,  $\kappa = -1/R$ .

A first idea is to simply truncate the series in (8) after  $N$  terms. For  $N \geq 3$  this leads to instability problems. It was, therefore, suggested in Barry et al. (1988) to modify the coefficient of the  $\Phi_1$  term in (8) by replacing  $s$  by  $(s + \delta)$ , thus introducing an arbitrary parameter  $\delta$ . Notice that the term  $(s + \delta)^{-1}$  corresponds in the time domain to a factor  $e^{-\delta t}$ ; therefore, the afore-

mentioned modification essentially amounts to an artificial increase of the damping properties of (8). The first three approximations are:

$$\hat{t} = \mu \hat{u}_v = -\frac{s\mu}{\beta} \hat{u} \text{ on } \Gamma_1 \dots \dots \dots (10a)$$

$$\hat{t} = \mu \hat{u}_v = -\frac{s\mu}{\beta} \hat{u} + \frac{1}{2} \kappa \mu \hat{u} \text{ on } \Gamma_1 \dots \dots \dots (10b)$$

$$\hat{t} = \mu \hat{u}_v = -\frac{s\mu}{\beta} \hat{u} + \frac{1}{2} \kappa \mu \hat{u} + \frac{\beta\mu}{s + \delta} \left( \frac{1}{2} \hat{u}_{\lambda\lambda} + \frac{1}{8} \kappa^2 \hat{u} \right) \text{ on } \Gamma_1 \dots \dots \dots (10c)$$

Translation back to the time domain yields:

$$\tau = \mu u_v = -\frac{\mu}{\beta} u_t \text{ on } \Gamma_1 \dots \dots \dots (11a)$$

$$\tau = \mu u_v = -\frac{\mu}{\beta} u_t + \frac{1}{2} \kappa \mu u \text{ on } \Gamma_1 \dots \dots \dots (11b)$$

$$\tau_t + \delta \tau = \mu u_{vt} + \delta \mu u_v = -\frac{\mu}{\beta} u_{tt} + \left( \frac{1}{2} \kappa - \frac{\delta}{\beta} \right) \mu u_t + \frac{1}{2} \beta \mu u_{\lambda\lambda} + \left( \frac{1}{8} \kappa^2 \beta + \frac{1}{2} \kappa \delta \right) \mu u \text{ on } \Gamma_1 \dots \dots \dots (11c)$$

We point out that the procedure yielding (8) is quite general and is exact in the sense that  $\mathcal{F}$  has an asymptotic expansion in powers of  $s^m$  for  $m = 1, 0, -1, -2, \dots$  [the first three terms,  $s, s^0$ , and  $s^{-1}$ , are given by (9)]. What is not determined is how one should choose the parameter  $\delta$ . An argument is given in Barry et al. (1988) to show that there is a minimum value  $\delta_{cr}$  of  $\delta$ , below which one may expect instability. In the case of an arbitrary boundary,  $\Gamma_1$ ,  $\delta_{cr} = -\bar{\kappa}^2/4\kappa$  where  $\bar{\kappa}, \kappa$  denote upper and lower bounds, respectively, for the curvature  $\kappa$ . Furthermore, as  $\delta$  tends to infinity, (11c) tends to (11b), which is expected to be less accurate. Thus one would anticipate that there is an optimal choice of  $\delta$ .

Eqs. (11a) and (11b) have a simple physical interpretation. The first condition corresponds to the well-known viscous boundary. It can be realized by attaching to the boundary  $\Gamma_1$  a set of distributed viscous dashpots of constant  $\mu/\beta$ , while the second condition, also well known for the particular case of a circle, consists of the same set of dashpots, in parallel with distributed springs of stiffness  $-(1/2)\kappa\mu$ . Eq. (11c) has also an interesting physical interpretation that will be discussed in the next section. Observe that while (11c) is not completely local as are (11a) and (11b), it involves only time and spatial derivatives up to second order.

It is worth noting that for  $\delta = -\beta\kappa$ , (11c) reduces to one derived by Kriegsmann et al. (1987). For the special case of a circle (11c) also reduces to one derived (by quite different methods) by Bayliss and Turkel (1980) provided one chooses  $\delta = 4\delta_{cr}$  where  $\delta_{cr} = \beta/(4R)$ . We remark that the special choice  $\delta = 4\delta_{cr}$  makes (10c) agree with (8) through terms of order  $s^{-2}$ . Thus, for problems involving higher frequencies, we expect the latter to be a good choice; this is illustrated in our experiments. However, it is also shown that it is not such a good choice if lower frequencies are dominant. Eqs. (11b) and (11c) also coincide with the Engquist and Majda (1977, 1979) conditions for the case of a half-space ( $\kappa \equiv 0$ ). A condition pertaining

to circular geometry is also presented in Engquist and Majda (1977) that again coincides with (11b). These authors, however, give no condition comparable to (11c).

The introduction of the approximate absorbing conditions [(11a)–(11c)] gives rise to a family of modified initial value problems defined over the annular region  $\Omega_2$  (Fig. 1). Each entails finding the displacement field  $u_N$  that satisfies the governing wave equation (1a) within  $\Omega_2$ , together with (1b) and (1c) as well as one of (11a)–(11c). The hope is that  $u_N$  will approximate the solution  $u$  of the original problem [(1) with  $u$  outgoing] within  $\Omega_2$  with increasing accuracy as  $N$  increases.

### DISCRETIZATION SCHEMES

In order to discretize the problem within  $\Omega_2$  using finite elements, the problem is first recast into a variational formulation. We illustrate with (11c) since the formulation with (11a) or (11b) is straightforward. In particular, the latter conditions lead to standard damping and stiffness matrices analogous to those for an elastic foundation. Multiply (1a) by a test function  $v$  and integrate over  $\Omega_2$  using the divergence theorem and (1b). This results in:

$$\mu \int_{\Omega_2} \nabla u \cdot \nabla v dx + \rho \int_{\Omega_2} v u_{,tt} dx = \tau_0 \int_{\Gamma} v p d\lambda + \int_{\Gamma_1} v \tau d\lambda \dots \dots \dots (12)$$

Next, multiply (11c) by a test function  $\chi$ , and integrate over  $\Gamma_1$ . For simplicity, from this point on we consider the case of a circular boundary  $\Gamma_1$  of radius  $r_2$  for which  $\kappa = -1/r_2$  is constant. This gives:

$$\int_{\Gamma_1} (\tau_t + \delta \tau) \chi d\lambda = -\frac{\mu}{\beta} \int_{\Gamma_1} u_{,tt} \chi d\lambda - \left( \frac{1}{2r_2} + \frac{\delta}{\beta} \right) \mu \int_{\Gamma_1} u_t \chi d\lambda - \frac{1}{2} \beta \mu \int_{\Gamma_1} u_{,\lambda} \chi_{,\lambda} d\lambda + \left( \frac{\beta}{8r_2^2} - \frac{\delta}{2r_2} \right) \mu \int_{\Gamma_1} u \chi d\lambda \dots \dots \dots (13)$$

In deriving the third term on the right-hand side of (13) use has been made of the fact that the curve  $\Gamma_1$  is closed. This eliminates the term that arises from integration by parts. Using the method of images, it can be shown, however, that (13) remains valid for a half plane, provided  $\Gamma_1$  is perpendicular to the free surface at the point of confluence. Special treatment would be required for a different geometry.

We consider  $\tau$  on  $\Gamma_1$  as an additional independent unknown. The problem, then, is to find the pair  $(u, \tau)$ , with  $u$  and  $\tau$  initially at rest, that satisfies (12) and (13) for all pairs of admissible functions  $(v, \chi)$ .

The spatial discretization of this problem involves using standard finite element piecewise polynomial approximations for the displacements in the closure  $\bar{\Omega}_2$  of  $\Omega_2$ , and tractions  $\tau$  on  $\Gamma_1$  and their respective test functions, as follows:

$$u(\mathbf{x}, t) \approx \Psi^T(\mathbf{x})\mathbf{u}(t); \quad v(\mathbf{x}) \approx \Psi^T(\mathbf{x})\mathbf{v} \dots \dots \dots (14a)$$

$$\tau(\mathbf{x}, t) \approx \Phi^T(\mathbf{x})\boldsymbol{\tau}(t); \quad \chi(\mathbf{x}) \approx \Phi^T(\mathbf{x})\boldsymbol{\chi} \dots \dots \dots (14b)$$

in which  $\Psi$  and  $\Phi$  = vectors of global shape functions;  $\mathbf{u}$  and  $\boldsymbol{\tau}$  = the unknown nodal displacements and tractions, defined over  $\bar{\Omega}_2$  and  $\Gamma_1$ , respectively, initially at rest; and  $\mathbf{v}$  and  $\boldsymbol{\chi}$  = arbitrary vectors of dimensions  $N_u$  and  $N_\tau$ , respectively. Introducing (14a) and (14b) into (12) and (13) and

requiring the corresponding equations to hold for arbitrary  $\mathbf{v}$  and  $\boldsymbol{\chi}$  results in the following equations:

$$\mathbf{M}\ddot{\mathbf{u}} + \mathbf{K}\mathbf{u} = \mathbf{p} + \mathbf{E}\boldsymbol{\tau} \dots\dots\dots (15a)$$

$$\mathbf{F}\boldsymbol{\tau} + \delta\mathbf{F}\boldsymbol{\tau} = -\frac{\mu}{\beta}\mathbf{E}^T\ddot{\mathbf{u}} - \left(\frac{1}{2r_2} + \frac{\delta}{\beta}\right)\mu\mathbf{E}^T\dot{\mathbf{u}} - \beta\mu\mathbf{G}\mathbf{u} + \left(\frac{\beta}{8r_2^2} - \frac{\delta}{2r_2}\right)\mu\mathbf{E}^T\mathbf{u} \dots\dots\dots (15b)$$

in which a superdot (·) denotes time derivative, and  $\mathbf{M}$  and  $\mathbf{K}$  are standard mass and stiffness symmetric matrices over  $\Omega_2$  whose entries are:

$$M_{ij} = \rho \int_{\Omega_2} \psi_i \psi_j d\mathbf{x}; \quad K_{ij} = \mu \int_{\Omega_2} \nabla\psi_i \cdot \nabla\psi_j d\mathbf{x} \dots\dots\dots (16a)$$

while  $\mathbf{p}$  is the effective load vector on  $\Gamma_1$  and  $\mathbf{E}$ ,  $\mathbf{F}$ , and  $\mathbf{G}$  are boundary matrices on  $\Gamma_1$ , given by

$$\mathbf{p} = \tau_0 \int_{\Gamma} \boldsymbol{\psi} p d\lambda; \quad \mathbf{E} = \int_{\Gamma_1} \boldsymbol{\psi} \boldsymbol{\phi}^T d\lambda; \quad \mathbf{F} = \int_{\Gamma_1} \boldsymbol{\phi} \boldsymbol{\phi}^T d\lambda; \\ \mathbf{G} = \int_{\Gamma_1} \boldsymbol{\phi}_\lambda \boldsymbol{\psi}_\lambda^T d\lambda \dots\dots\dots (16b)$$

The use of the mixed variational procedure, with  $\boldsymbol{\tau}$  on  $\Gamma_1$  as an unknown, eliminates the necessity of calculating the normal derivatives of  $u$  at  $\Gamma_1$ . This seems preferable to finite differences.

Various step-by-step techniques can be used to solve (15a) and (15b) with associated vanishing initial conditions. For instance, one approach is to evaluate (15a) at time step  $(r + 1)$ , combined with Newmark's trapezoidal method, while evaluating (15b) at  $[r + (1/2)]$  in combination with central differences [just taking backward differences in (15b) at  $(r)$  led to an unstable scheme]. This results in:

$$\mathbf{M}\ddot{\mathbf{u}}^{r+1} + \mathbf{K}\mathbf{u}^{r+1} - \mathbf{E}\boldsymbol{\tau}^{r+1} = \mathbf{p}^{r+1} \dots\dots\dots (17a)$$

$$\mathbf{u}^{r+1} = \mathbf{u}^r + \dot{\mathbf{u}}^r \Delta t + \frac{\ddot{\mathbf{u}}^r + \ddot{\mathbf{u}}^{r+1}}{4} (\Delta t)^2 \dots\dots\dots (17b)$$

$$\dot{\mathbf{u}}^{r+1} = \dot{\mathbf{u}}^r + \frac{\ddot{\mathbf{u}}^r + \ddot{\mathbf{u}}^{r+1}}{2} \Delta t \dots\dots\dots (17c)$$

$$\mathbf{F} \frac{\boldsymbol{\tau}^{r+1} - \boldsymbol{\tau}^r}{\Delta t} + \delta\mathbf{F} \frac{\boldsymbol{\tau}^{r+1} + \boldsymbol{\tau}^r}{2} = -\frac{\mu}{\beta}\mathbf{E}^T \frac{\ddot{\mathbf{u}}^{r+1} + \ddot{\mathbf{u}}^r}{2} - \left(\frac{1}{2r_2} + \frac{\delta}{\beta}\right)\mu\mathbf{E}^T \frac{\mathbf{u}^{r+1} - \mathbf{u}^r}{\Delta t} \\ - \frac{1}{2}\beta\mu\mathbf{G} \frac{\mathbf{u}^{r+1} + \mathbf{u}^r}{2} + \left(\frac{\beta}{8r_2^2} - \frac{\delta}{2r_2}\right)\mu\mathbf{E}^T \frac{\mathbf{u}^{r+1} + \mathbf{u}^r}{2} \dots\dots\dots (17d)$$

This is a system of simultaneous equations for  $\ddot{\mathbf{u}}^{r+1}$ ,  $\dot{\mathbf{u}}^{r+1}$ ,  $\mathbf{u}^{r+1}$ , and  $\boldsymbol{\tau}^{r+1}$  that may be solved, e.g., by eliminating  $\mathbf{u}^{r+1}$ ,  $\dot{\mathbf{u}}^{r+1}$ , and  $\boldsymbol{\tau}^{r+1}$  using the last three equations, and then solving (17a) for  $\ddot{\mathbf{u}}^{r+1}$ .

An alternative approach for solving (15a) and (15b) is to use central differences for (15a)

$$\frac{\mathbf{M}}{2(\Delta t)^2} (\mathbf{u}^{r+1} - 2\mathbf{u}^r + \mathbf{u}^{r-1}) + \mathbf{K}\mathbf{u}^r = \mathbf{p}^r + \mathbf{E}\boldsymbol{\tau}^r \dots\dots\dots (18)$$

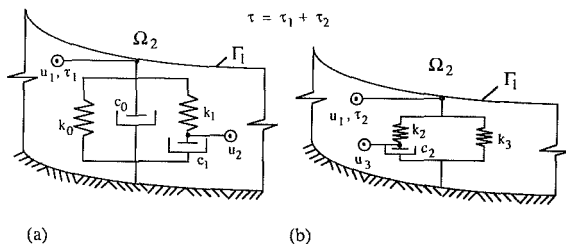


**FIG. 2. Mechanical Interpretation of Viscoelastic Absorbing Boundary Condition Given by (11c) or, Equivalently, by (24) and (25): (a) Uncoupled Distributed Maxwell Shear Elements; (b) Shear Layer with Coupled Standard Linear Solid Elements**

in combination with (17d). The first approach has the advantage of being unconditionally stable for a prescribed  $\tau$ . The second one, however, while only conditionally stable, uncouples the solution of  $\mathbf{u}^{r+1}$  from that of  $\tau^{r+1}$ . One may solve first (18) for  $\mathbf{u}^{r+1}$  using the known vector  $\mathbf{E}\tau^r$  as an effective load on  $\Gamma_1$  and then solve (17d) to determine the updated traction  $\tau^{r+1}$ .

**Local Boundary Elements**

While the two numerical procedures just described are easy to implement in the computer using *ad hoc* software and can be extended to more general problems, they cannot be used readily with existing general purpose finite element packages. It is of interest that an alternative procedure can be developed for incorporating the absorbing boundary condition, (11c), into standard algorithms developed originally for handling only interior problems. This may be accomplished by rewriting (11c) into an equivalent form that avoids the time derivative of the traction, at the expense of introducing two auxiliary displacements on the absorbing boundary  $\Gamma_1$ . Let  $u_1$  be the actual displacement  $u$  on  $\Gamma_1$  and  $u_2, u_3$  the auxiliary displacements. It can, then, be readily verified that the traction  $\tau$  on  $\Gamma_1$  can be decomposed into two components  $\tau_1$  and  $\tau_2$ , defined by:

$$\tau_1 = k_0 u_1 + c_0 \dot{u}_1 + k_1(u_1 - u_2) \dots \dots \dots (19a)$$

$$\tau_2 = -k_3 u_1'' - k_2(u_1'' - u_3'') \dots \dots \dots (19b)$$

in which  $u_2$  and  $u_3$  are related to  $u_1$  by:

$$k_1(u_1 - u_2) = c_1 \dot{u}_2 \dots \dots \dots (19c)$$

$$k_2(u_1'' - u_3'') = c_2 \dot{u}_3'' \dots \dots \dots (19d)$$

A prime (') denotes tangential derivative and the constants  $k_0, k_1, k_2, k_3, c_0, c_1,$  and  $c_2$  are given by:

$$k_0 = -\left(\frac{1}{8} \kappa^2 \beta + \frac{1}{2} \kappa \delta\right) \frac{\mu}{\delta}; \quad c_0 = \frac{\mu}{\beta}; \quad k_1 = \frac{\kappa^2 \beta \mu}{8 \delta} \dots \dots \dots (20a)$$

$$c_1 = \frac{\kappa^2 \beta \mu}{8 \delta^2}; \quad k_2 = -k_3 = \gamma k_1; \quad c_2 = \gamma c_1; \quad \gamma = -\frac{4}{\kappa^2} \dots \dots \dots (20b)$$

Eqs. (19a)–(19d) have an interesting mechanical interpretation, which is depicted in Fig. 2. As shown in Fig. 2(a), which corresponds to (19a) and (19c),  $\tau_1$  is the traction generated on  $\Gamma_1$  due to a distributed, but uncoupled,

generalized Maxwell shear model;  $k_0$ ,  $k_1$  and  $c_0$ ,  $c_1 =$  stiffness and damping constants; and  $u_2 =$  the displacement of the intermediate node in the Maxwell element. Similarly, corresponding to (19*b*) and (19*d*),  $\tau_2$ , as shown in Fig. 2(*b*), is the traction on  $\Gamma_1$  due to a shear layer consisting of a coupled distributed standard linear solid. The entire assembly in Figs. 2(*a*) and 2(*b*) may be viewed as a generalized damped Pasternak foundation (Kerr 1964). This mechanical interpretation is perhaps more useful for purposes of numerical discretization than for the actual construction of a physical absorbing boundary using the spring and damping constants defined by (20*a*) and (20*b*), since some of these constants are negative and thus the individual springs and dashpots are not physically realizable. If one wishes to construct an actual physical absorbing boundary to simulate an exterior infinite domain one may deal directly with (19*a*)–(19*d*) or (11*a*)–(11*c*) or with their Laplace or Fourier transforms, and design an absorbing system consisting of a viscoelastically damped Winkler model (Kerr 1964) in parallel with a viscoelastic shear layer with the required relaxation function.

The spatially discretized version of this alternative formulation of the absorbing boundary condition is obtained by approximating  $u_1$  and  $u_2$ , as well as their corresponding test functions  $v_1$  and  $v_2$  by piecewise polynomials:

$$u_i(\mathbf{x}, t) = \boldsymbol{\sigma}^T(\mathbf{x})\mathbf{u}_i(t); \quad v_i(\mathbf{x}) = \boldsymbol{\sigma}^T(\mathbf{x})\mathbf{v}_i \text{ on } \Gamma_1 \text{ for } i = 1, 2 \dots \dots \dots (21)$$

in which  $\boldsymbol{\sigma}(\mathbf{x})$ , the global shape functions for the displacements  $\mathbf{u}$  on  $\Gamma_1$ , corresponds to the restriction to  $\Gamma_1$  of  $\boldsymbol{\psi}(\mathbf{x})$  in (14*a*). On the other hand, since from (19*d*)  $u_3$  and  $u_1$  are related only through their second tangential derivatives, we express the tangential derivative of  $u_3$  and its test function via:

$$u'_3(\mathbf{x}, t) = \boldsymbol{\zeta}^T(\mathbf{x})\mathbf{w}_3(t); \quad v'_3(\mathbf{x}) = \boldsymbol{\zeta}^T(\mathbf{x})\mathbf{v}_3 \text{ on } \Gamma_1 \dots \dots \dots (22)$$

rather than approximating  $u_3$  directly, in order to avoid singular matrices in later calculations. After multiplying the equation:

$$\tau = \tau_1 + \tau_2 \dots \dots \dots (23)$$

by the test function  $v_1$ , with  $\tau_1$  and  $\tau_2$  given by (19*a*) and (19*b*); (19*c*) by  $v_2$ ; (19*d*) by  $v_3$ ; substituting (21) and (22) into the resulting equations; integrating over  $\Gamma_1$ ; making use of (20*a*) and (20*b*), and noting that  $\mathbf{v}_1$ ,  $\mathbf{v}_2$ , and  $\mathbf{v}_3$  are arbitrary, there results the following counterpart of (15*b*):

$$\begin{pmatrix} \mathbf{T} \\ 0 \\ 0 \end{pmatrix} = \begin{bmatrix} (\beta^2/2r_2)\mathbf{m}_1 & -(\beta/8\delta r_2^2)\mathbf{m}_1 & (\beta/2\delta)\mathbf{k} \\ -(\beta^3/8\delta r_2^2)\mathbf{m}_1 & (\beta^3/8\delta r_2^2)\mathbf{m}_1 & 0 \\ (\beta/2\delta)\mathbf{k}^T & 0 & -(\beta^3/2\delta)\mathbf{m}_2 \end{bmatrix} \begin{pmatrix} \mathbf{u}_1 \\ \mathbf{u}_2 \\ \mathbf{w}_3 \end{pmatrix} + \begin{bmatrix} \beta\mathbf{m}_1 & 0 & 0 \\ 0 & (\beta^3/8\delta^2 r_2^2)/\mathbf{m}_1 & 0 \\ 0 & 0 & -(\beta^3/2\delta^2)\mathbf{m}_2 \end{bmatrix} \begin{pmatrix} \dot{\mathbf{u}}_1 \\ \dot{\mathbf{u}}_2 \\ \dot{\mathbf{w}}_3 \end{pmatrix} \dots \dots \dots (24)$$

in which

$$\begin{aligned} \mathbf{T} &= \int_{\Gamma_1} \boldsymbol{\sigma} \tau d\lambda; & \mathbf{m}_1 &= \rho \int_{\Gamma_1} \boldsymbol{\sigma} \boldsymbol{\sigma}^T d\lambda; \\ \mathbf{m}_2 &= \rho \int_{\Gamma_1} \boldsymbol{\zeta} \boldsymbol{\zeta}^T d\lambda; & \mathbf{k} &= \mu \int_{\Gamma_1} \boldsymbol{\sigma}' \boldsymbol{\zeta}^T d\lambda \dots \dots \dots (25) \end{aligned}$$

In (24),  $\mathbf{T} =$  the nodal tractions on  $\Gamma_1$ , while  $\mathbf{u}_1$ ,  $\mathbf{u}_2$ , and  $\mathbf{w}_3$  are the cor-

responding values of the displacements  $u_1(u)$ ,  $u_2$ , and the tangential derivative  $u_3'$ .

It can be clearly seen from (24) that the absorbing boundary condition (11c) can be taken into consideration by merely adding the *symmetric* stiffnesslike and dampinglike contributions indicated in (24) to the standard finite element semidiscretized equations for the interior region. All that is required is to include the additional boundary degrees of freedom  $u_2$  and  $w_3$  corresponding to the auxiliary variables  $u_2$  and  $u_3'$  shown in Fig. 2. Since  $u_1$ ,  $u_2$ , and  $u_3'$  are approximated by piecewise polynomials on  $\Gamma_1$ , and only second-order spatial derivatives are involved in (19), as is the case for the governing wave equation in  $\Omega_2$ , then each boundary element will be coupled only to its neighboring elements. As far as the implementation is concerned, the boundary condition given by (24) appears as one more layer of ordinary finite elements, with modified stiffness and damping matrices, thereby avoiding the need for any special treatment. Should the geometry of the absorbing boundary  $\Gamma_1$  be other than circular, the coefficients of the various element matrices in (24) would be different (the curvature would no longer be constant); however, the overall structure of the matrices would still be retained. This formulation, which naturally can be applied directly in the time domain or in the frequency domain, allows for the solution of problems in infinite domains with localized nonlinearities (e.g., if the cavity were filled with inelastic material), using the viscoelastic boundary with existing finite element packages.

## NUMERICAL RESULTS

This section describes the results of numerical experiments conducted in order to assess the accuracy of the approximate absorbing boundary conditions and of their discretized versions presented in the preceding section. The numerical results will also serve to develop rules for determining the minimum radius at which these absorbing boundaries should be placed to ensure their satisfactory performance. Two types of calculations will be performed. One consists in obtaining exact solutions for the approximate problems that result from the introduction of the various artificial boundary conditions and in comparing these solutions with those corresponding to the original problem defined over the infinite domain  $\Omega$ . These comparisons will permit examining the performance of the artificial absorbing boundaries without contamination from discretization errors. Examples involving the step-by-step solution of the spatially discretized equations of motion will be presented subsequently to illustrate the adequacy of the discretization schemes for the absorbing boundary given by (17a)–(17d) and (24). The central difference technique [(18)] has not yet been implemented. A circular cavity and a concentric circular artificial boundary will be considered throughout to facilitate the derivation of exact solutions. Thus, the computational domain  $\Omega_2$  will be an annulus with inner and outer boundaries,  $\Gamma$  and  $\Gamma_1$ , of radius  $r_1$  and  $r_2$ , respectively. The response of the system to both steady-state and transient excitations will be examined next.

As a step towards gaining insight into the effect of the various absorbing boundaries on the system response under arbitrary excitation we start by considering a Fourier analysis involving the response due to an applied traction on  $\Gamma$  of the form:

$$\tau = \mu u_r = \tau_0 \cos n\theta e^{i\omega t}, \quad n = 0, 1, 2, \dots \text{ on } \Gamma \dots \dots \dots (26)$$

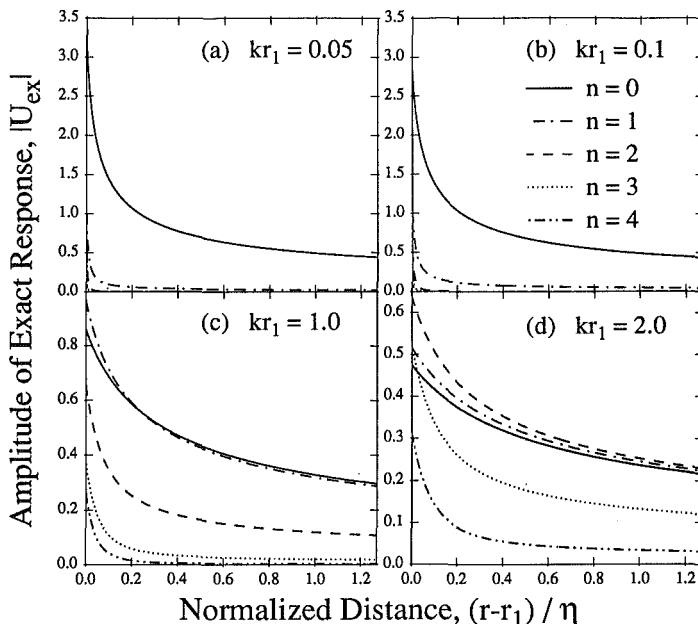


**FIG. 3. Exact Steady-State Response within Infinite Medium due to Harmonic Excitation: (a)  $kr_1 = 0.05$ ; (b)  $kr_1 = 0.1$ ; (c)  $kr_1 = 1.0$ ; (d)  $kr_1 = 2.0$**

in which  $\theta$  = the angular polar coordinate and  $\omega$  = the circular frequency of excitation. Each approximate problem then entails solving (1a) in  $\Omega_2$  subject to (26) and one of the absorbing boundary conditions given by (11a), (11b), and (11c). These three approximate problems, as well as the exact one, have closed-form exact solutions of the form:

$$u(r, \theta, t) = U(r) \cos n\theta e^{i\omega t}, \quad n = 0, 1, 2, \dots \text{ in } \Omega_2 \dots \dots \dots (27)$$

The corresponding expressions for  $U(r)$ ,  $U_{app}(r)$ , and  $U_{ex}(r)$ , for the approximate and the exact problems, are given in Appendix I. The approximate and the corresponding exact solutions will be compared for several positions of the absorbing boundaries, angular modes  $n$ , and frequency of excitation  $\omega$ . Naturally, only differences in the various functions  $U(r)$  need be examined.

For future reference we present in Fig. 3 the normalized amplitude of the displacement  $U_{ex}$  corresponding to the exact problem defined over  $\Omega$ , as a function of the distance  $r - r_1$ , normalized with respect to the wave length  $\eta$ , for several frequencies and angular modes. The following quantities are used in this and subsequent figures:

$$kr_1 = \frac{\omega r_1}{\beta}; \quad \eta = \frac{2\pi}{\omega} \beta; \quad U_0 = \frac{\tau_0 r_1}{\mu}; \quad t_0 = \frac{r_1}{\beta} \dots \dots \dots (28)$$

in which  $k$  = the wave number,  $\eta$  = the wavelength, and  $U_0$  and  $t_0$  = a reference displacement and time, respectively. From Fig. 3 one observes that: (1) The amplitude of  $U_{ex}$  decreases with frequency and, even more rapidly, with distance; (2) the peak amplitude of the displacement corre-

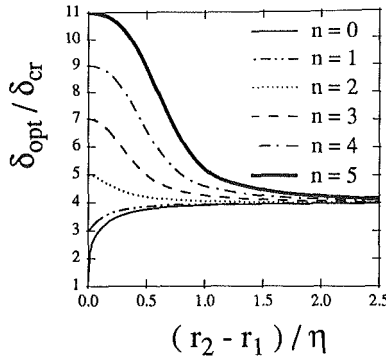


**FIG. 4. Optimum Value of  $\delta$  in Viscoelastic Boundary Condition to Minimize Error of Steady-State Response**

sponding to the symmetric cylindrical case ( $n = 0$ ) decreases with increasing frequency; and (3) for a fixed frequency, the amplitude of  $U_{ex}$  at a given point in  $\Omega$  decreases with increasing  $n$  beyond a certain value of  $n$  [e.g.,  $n > 2$  for  $kr_1 = 2$  in Fig. 3(d)]. These characteristics of the solution of the exact problem will be useful later in explaining the performance of the absorbing boundaries.

Before analyzing the errors incurred by the use of the approximate boundary conditions, we recall that (11c) includes a stabilizing parameter  $\delta$  introduced to prevent exponential error growth. Except for the requirement that it satisfy the lower bound  $\delta \geq \delta_{cr}$ , this parameter is arbitrary. Due to the availability of the analytic solution for  $U(r)$ ,  $\delta$  can be chosen to minimize the difference between the solutions  $U_{app}$  and  $U_{ex}$  to the approximate and exact problems. Details of the procedure are given by Kallivokas (1990). The corresponding values of  $\delta$ , herein denoted as  $\delta_{opt}$ , are functions of distance and frequency through the parameter  $(r_2 - r_1)/\eta$ , as well as of the mode  $n$ , as shown in Fig. 4. For small values of the distance from the absorbing boundary to the cavity, relative to the wavelength,  $\delta_{opt}$  tends to the limit:

$$\lim_{(r_2 - r_1)/\eta \rightarrow 0} \delta_{opt} = (2n + 1)\delta_{cr} = (2n + 1) \frac{\beta}{4r_2} \dots \dots \dots (29)$$

which depends on the angular mode  $n$ , while for large values of this parameter,  $\delta_{opt}$  tends to a constant equal to  $4\delta_{cr}$ . [We recall this is the Bayliss and Turkel (1980) value.] The approach to this limit is fast for  $n = 0$  and  $n = 1$ , but becomes slower as  $n$  increases. If a constant value of  $\delta = 4\delta_{cr}$  is used in the calculations one then may expect increasing errors at small frequencies and distances with increasing  $n$ .

**Exact Analysis**

To examine the accuracy of the three approximate absorbing conditions [(11a)–(11c)], the relative error:

$$E(r_1) = \frac{|U_{ex}(r_1) - U_{app}(r_1)|}{|U_{ex}(r_1)|} \dots \dots \dots (30)$$

in the displacement at the inner boundary has been calculated for each boundary

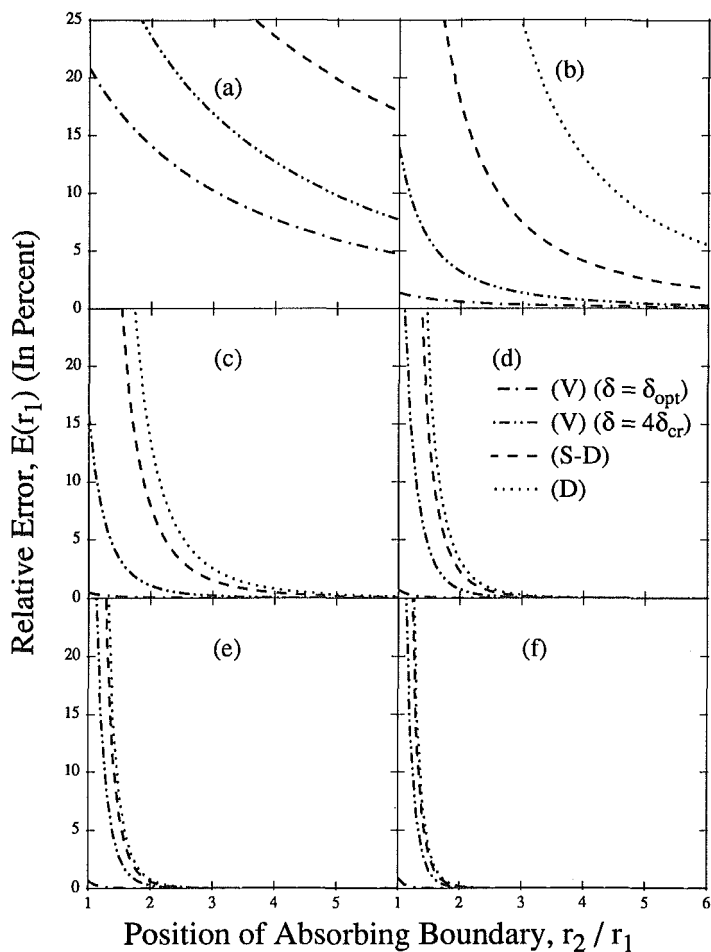


**FIG. 5. Relative Error at Inner Boundary as Function of  $r_2/r_1$  due to Various Absorbing Boundaries;  $kr_1 = 0.05$ ; (a)  $n = 0$ ; (b)  $n = 1$ ; (c)  $n = 2$ ; (d)  $n = 3$ ; (e)  $n = 4$ ; (f)  $n = 5$**

condition versus  $r_2/r_1$ , as shown in Figs. 5 and 6, for the first six angular modes, and for two frequencies of excitation  $kr_1$ , a low value of 0.05 and a higher one of 0.5. In what follows, (11a), (11b), and (11c) also will be referred to as the dashpot (*D*), spring-dashpot (*S-D*), and spatially coupled viscoelastic (*V*) boundaries, respectively. For the latter, results are presented for both  $\delta = \delta_{opt}$  and  $\delta = 4\delta_{cr}$ . In all cases the errors decrease with the order of the approximation; that is, for a fixed frequency and position of the absorbing boundary, one immediately observes an increasing goodness of fit in moving successively from the dashpot to the spring-dashpot, to the viscoelastic boundary. Conversely, for a given tolerance, the viscoelastic boundary requires a smaller buffer zone. As an example consider the case  $kr_1 = 0.5$ ,  $n = 0$ , and a desirable error of less than 5%. According to Fig. 6, one need

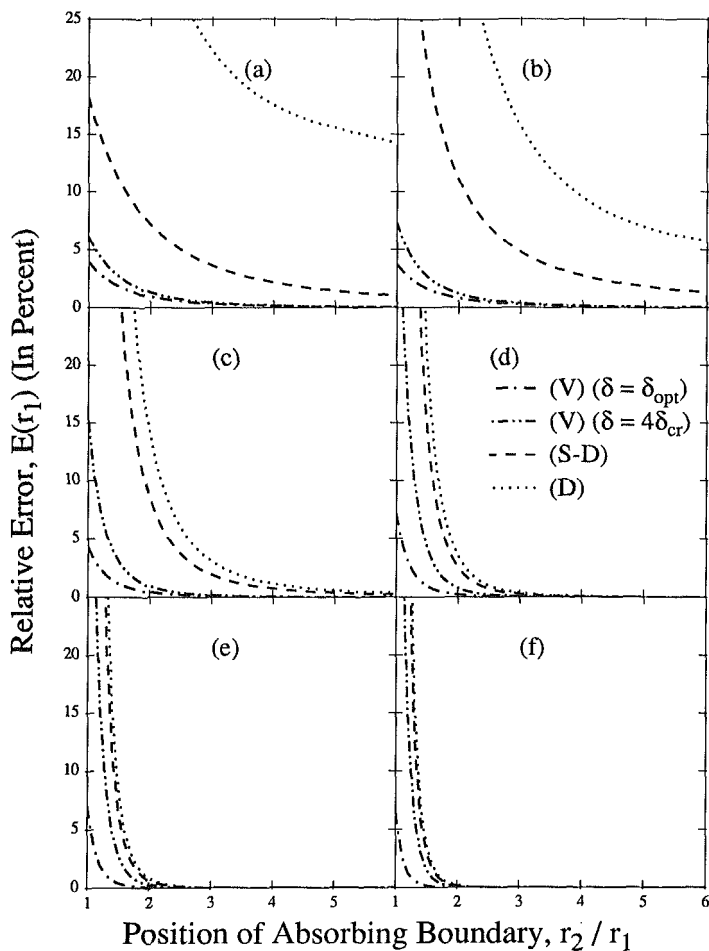


**FIG. 6. Relative Error at Inner Boundary as Function of  $r_2/r_1$  due to Various Absorbing Boundaries;  $kr_1 = 0.5$ : (a)  $n = 0$ ; (b)  $n = 1$ ; (c)  $n = 2$ ; (d)  $n = 3$ ; (e)  $n = 4$ ; (f)  $N = 5$**

only place the viscoelastic boundary at  $r_2 > 1.1r_1$ , whereas the dashpot-spring boundary requires  $r_2 > 2.5r_1$ , and the dashpot,  $r_2 > 16r_1$  (not shown due to the scale). These differences decrease at higher frequencies but become more pronounced at lower ones. Additional observations from Figs. 5 and 6 include: (1) Errors for a given boundary condition decrease with increasing frequency; (2) the errors are largest for the axisymmetric case ( $n = 0$ ) and decrease uniformly with  $n$ ; (3) while, as expected, accuracy increases with distance  $r_2/r_1$ , the rate of decay of the error is highly dependent on the angular mode (in fact, for  $n = 0$  and small frequencies, the widely used dashpot condition yields unacceptable results unless the boundary is placed very far); (4) as predicted by Fig. 4, using  $\delta = \delta_{opt}$  instead of  $4\delta_{cr}$  improves significantly the performance of the viscoelastic boundary when it

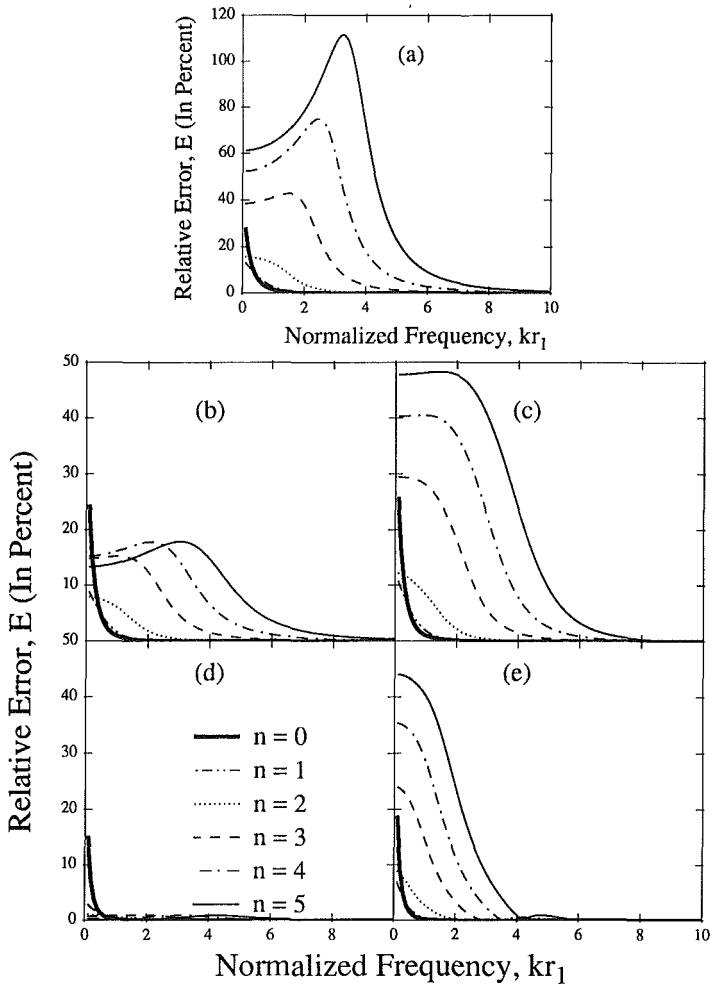


**FIG. 7. Relative Errors at Inner and Outer Boundaries as Function of Frequency  $kr_1$  due to Viscoelastic Boundary ( $\delta = 4\delta_{cr}$ ): (a)  $r_2/r_1 = 1.0$ ; (b)  $r_2/r_1 = 1.2$  (Error on  $r_1$ ); (c)  $r_2/r_1 = 1.2$  (Error on  $r_2$ ); (d)  $r_2/r_1 = 2.0$  (Error on  $r_1$ ); (e)  $r_2/r_1 = 2.0$  (Error on  $r_2$ )**

is placed near the cavity (the improvement is greatest for the lower frequency of excitation); and (5) whereas  $\delta_{opt}$  can be used to advantage in frequency-domain analyses and in time-domain calculations based on the FFT, it would, unfortunately, not be as practical for direct calculations in the time domain, since its frequency dependence would introduce convolutions into (11c).

To further examine the sensitivity of the viscoelastic boundary with  $\delta = 4\delta_{cr}$  to the frequency of excitation, Fig. 7 depicts the relative error,  $E$ , at both the inner and outer boundaries versus  $kr_1$  for several angular modes and positions of the absorbing boundary,  $\Gamma_1$ . One key observation is that the errors become very small at high frequencies, even if  $\Gamma_1$  coincides with the

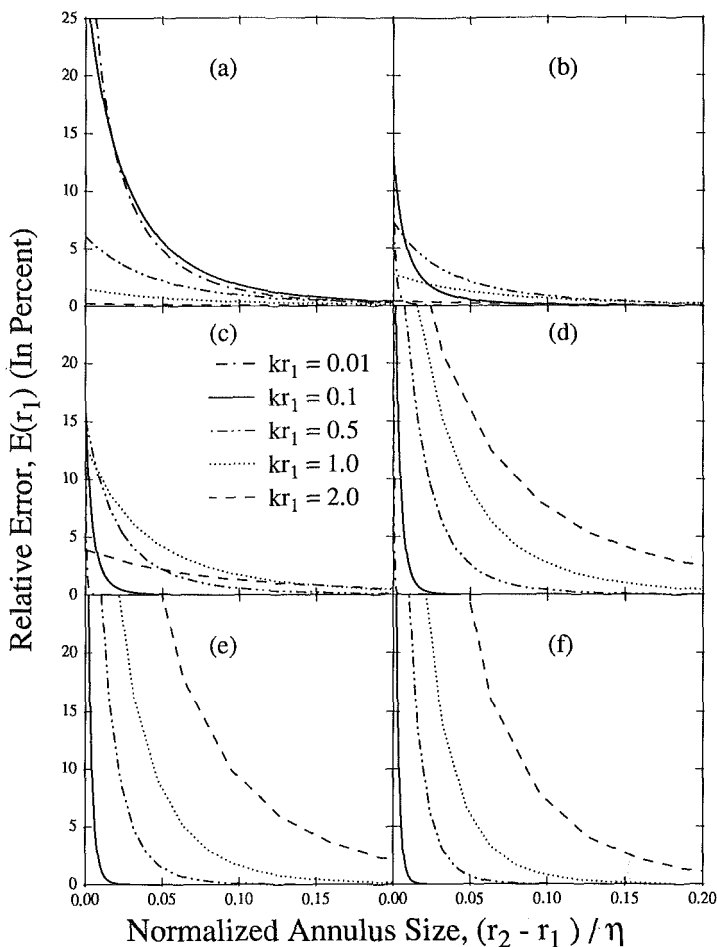


**FIG. 8. Relative Error at Inner Boundary as Function of Distance Wavelength Ratio for Different Frequencies of Excitation; Viscoelastic Boundary ( $\delta = 4\delta_{cr}$ ): (a)  $n = 0$ ; (b)  $n = 1$ ; (c)  $n = 2$ ; (d)  $n = 3$ ; (e)  $n = 4$ ; (f)  $n = 5$**

inner boundary  $\Gamma$ . This is to be expected since the present approach is based on ideas from geometrical optics [(6a) and (6b)]. At lower frequencies the error on  $\Gamma_1$  increases significantly, requiring that  $\Gamma_1$  be moved some distance away from  $\Gamma$ . While the errors on  $\Gamma_1$  decrease as the distance between these two boundaries increases, they remain significant even at  $r_2/r_1 = 2$  for  $n > 3$ . Fortunately, the effect of these errors on the inner boundary is negligible since the amplitude of the actual displacement for the higher angular modes decreases rapidly with distance, as discussed earlier in connection with Fig. 3.

In an effort to develop rules for determining the minimum radius  $r_2$  required for the viscoelastic boundary to limit the error on  $\Gamma$  to a desired value,  $E(r_1)$  is plotted in Fig. 8 versus  $(r_2 - r_1)/\eta$  for different values of  $n$  and

$kr_1$ . For the symmetric case ( $n = 0$ ) the low frequencies govern the location of  $\Gamma_1$ . Thus, to limit the error to 5% it is sufficient to place the viscoelastic boundary at a distance of  $0.06\eta$  from  $\Gamma$ , and at  $0.2\eta$  for an error of less than 1%. As  $n$  increases, errors at the higher frequencies become greater than for the low frequencies for a fixed value of the abscissa. The explanation to this paradox is that for a fixed  $(r_2 - r_1)/\eta$  the actual distance  $r_2 - r_1$  is inversely proportional to the normalized frequency  $kr_1$ . Thus, for example, a point on the  $kr_1 = 0.1$  curve corresponds to an actual physical distance of the artificial boundary, which is five times greater than the point with the same abscissa on the  $kr_1 = 0.5$  curve. Hence, in practice, selecting the position of  $\Gamma_1$  based on the lower dominant frequencies and  $n = 0$  can be expected to give satisfactory results for all frequencies and angular modes. This is confirmed by Fig. 9, which shows the transient displacement  $U$  at the inner and outer boundaries, when  $\Gamma_1$  is placed quite close to  $\Gamma$ , at  $r_2 = 1.2r_1$ , due to a rectangular pulse excitation of the form:

$$\tau = \mu u_r = \tau_0 \cos n\theta [H(t) - H(t - t_0)], \quad n = 0, 1, 2, \dots \text{ on } \Gamma \dots \dots (31)$$

in which  $H(t)$  = the Heaviside step pulse and  $t_0$  = the reference time defined in (28). This excitation represents a very severe test for the approximate absorbing boundaries since it contains large low-frequency contributions, including a strong zero-frequency component. Fig. 9, obtained using the fast Fourier transform (FFT) to transform the response from the frequency domain into the time domain, demonstrates that using dashpots to absorb outgoing waves is totally unacceptable when the artificial boundary is placed near the source and the excitation has strong low-frequency components. The spring-dashpot combination gives improved results, but these deteriorate with increasing  $n$  due to this boundary's inability to capture the angular variability of the response. The viscoelastic boundary, on the other hand, simulates quite successfully the actual response. Only some error for the very low frequency (long-time) components of the axially symmetric ( $n = 0$ ) mode is introduced with  $\delta = 4\delta_{cr}$ , while the results with  $\delta = \delta_{opt}$  are even better.

### Finite Element Analysis

The cavity was again subjected to the rectangular pulse (31) but this time the problem was solved by the finite element method, directly in the time domain. The aim was to examine the effect of the discretization of the viscoelastic boundary (with  $\delta = 4\delta_{cr}$ ) on the response, when this boundary is placed near the cavity ( $r_2 = 1.2r_1$ ), as before. Using eight-noded isoparametric quadrilateral elements the annulus was divided into four angular sectors and a single radial element. The absorbing boundary was also discretized by quadratic elements and numerical solutions were carried out for a time step  $\Delta t/t_0 = 0.01$  both with the mixed formulation represented by (17a)–(17d), and with the simple local boundary elements defined by (24). The resulting displacements at the inner and outer boundaries, for  $n = 0, 1, 2$  and  $\theta = 0$  are graphically indistinguishable from those obtained with the FFT from the corresponding exact frequency-domain solutions, which are shown by dashed-double dotted lines in Fig. 9. Hence, they are not plotted separately.

To further assess the accuracy of the new local boundary element, the response to three cycles of a low-frequency ( $kr_1 = 0.05$ ) sinusoidal excitation was considered in addition to that of the rectangular pulse. Following the recommendation drawn from Fig. 8, the absorbing boundary was placed far from the cavity, at a distance  $r_2 = 8.5r_1$ , corresponding to  $0.06\eta$ , for an

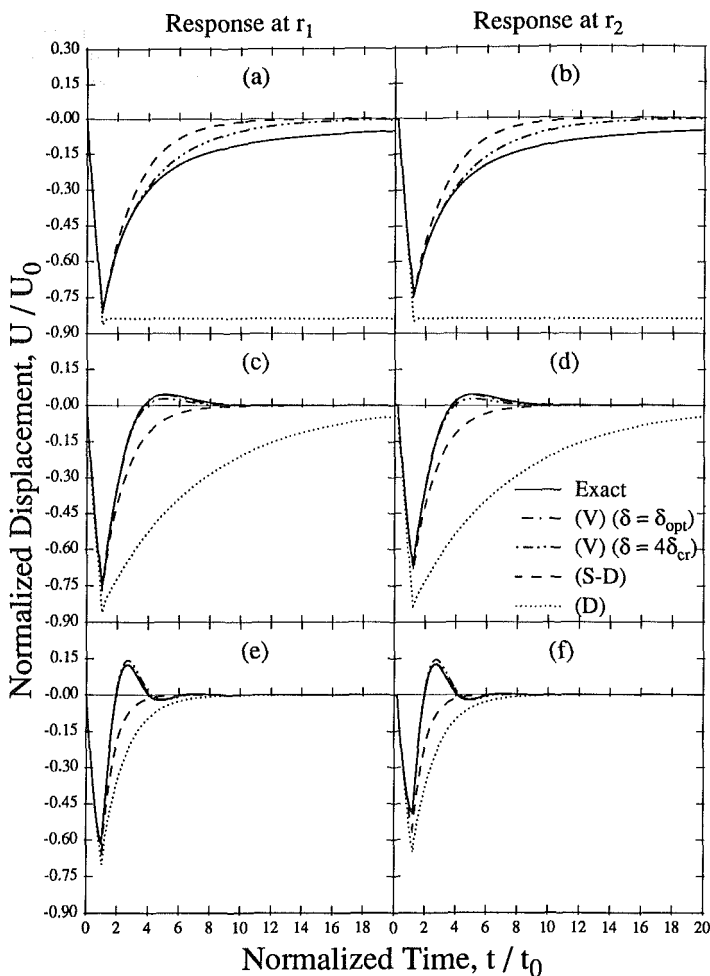


**FIG. 9. Effect of Various Absorbing Boundary Conditions on Transient Response due to Square-Pulse Excitation of Duration  $t/t_0 = 1$ ;  $r_2/r_1 = 1.2$ : (a)  $n = 0$  (Response at  $r_1$ ); (b)  $n = 0$  (Response at  $r_2$ ); (c)  $n = 1$  (Response at  $r_1$ ); (d)  $n = 1$  (Response at  $r_2$ ); (e)  $n = 2$  (Response at  $r_1$ ); (f)  $n = 2$  (Response at  $r_2$ )**

expected error of 5%. The actual error in the peak displacement between the approximate and the exact solution for  $n = 0$  is a surprisingly low 0.3%. Corresponding calculations for the spring-dashpot and dashpot boundaries exhibited 3% and 45% errors at the peak displacements. Fig. 10 shows the displacement at  $r_1$  and  $r_2$ , corresponding to  $\theta = 0$ , for one and two equally spaced radial elements and four angular sectors. It is noteworthy that even though the absorbing boundary is not close to the cavity, one or two radial elements are sufficient to obtain a highly accurate response for the symmetric angular mode, and acceptable for higher ones. That this should not be surprising can be inferred from Fig. 3, which shows that the exact response

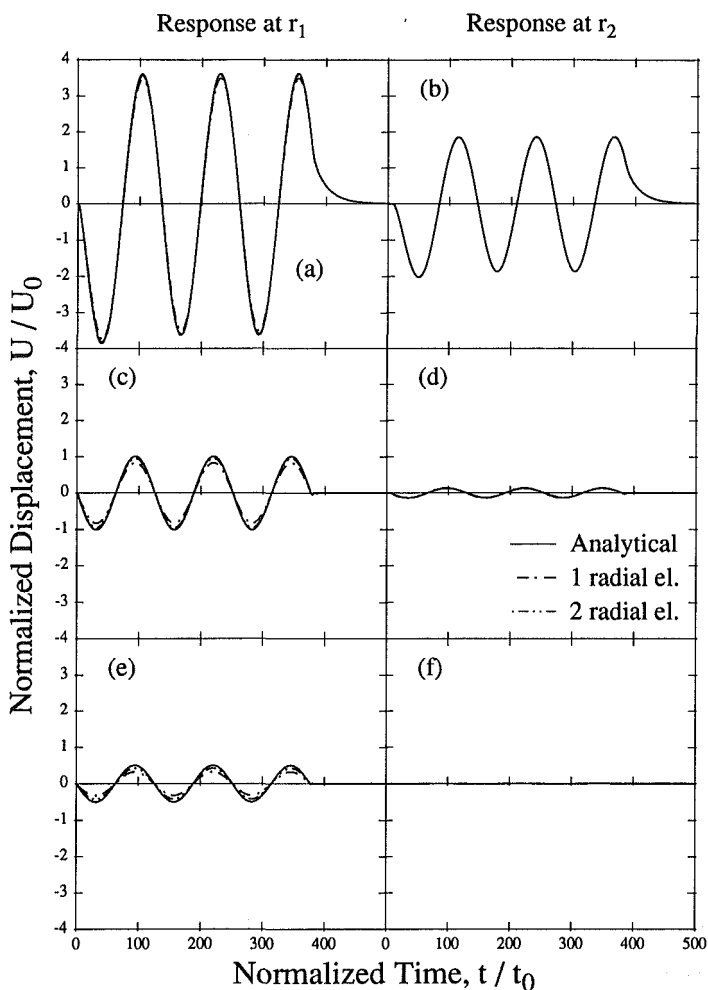


**FIG. 10. Effect of Viscoelastic Boundary ( $\delta = 4\delta_{cr}$ ) on Transient Response due to Low Frequency ( $kr_1 = 0.05$ ) Sinusoidal Excitation Calculated by Finite Element Method: (a)  $n = 0$  (Response at  $r_1$ ); (b)  $n = 0$  (Response at  $r_2$ ); (c)  $n = 1$  (Response at  $r_1$ ); (d)  $n = 1$  (Response at  $r_2$ ); (e)  $n = 2$  (Response at  $r_1$ );  $n_2 = 2$  (Response at  $r_2$ )**

decays monotonically with distance from the cavity, and, hence, can be approximated with just a few elements over a long distance. Since the effect of the symmetric mode is often predominant, one or two elements in the radial direction will be sufficient in many applications. Fig. 3 shows, in addition, that this observation will also apply in general at higher frequencies. Evidently, if the contribution of a higher angular mode is large, then a smaller mesh size in the radial direction, as well as in the angular direction, will be required at high frequencies.

**CONCLUSIONS**

1. Among the absorbing conditions examined herein, the viscoelastic boundary with  $\delta = 4\delta_{cr}$  is the most useful for direct calculations in the time domain. Its implementation, by means of the new symmetric, local, boundary element, or its alternative mixed method formulation, is essentially no more difficult and involves no more computational effort than the dashpot or spring-dashpot boundaries, yet it leads to a significant increase in accuracy. Conversely, for a given tolerance, the viscoelastic boundary requires a smaller buffer zone. Thus, to limit the error to 5% it is sufficient to place the viscoelastic boundary at a distance of 0.06 of the wavelength  $\eta$  from the region of physical interest, and at 0.2 $\eta$  for an error of less than 1%. One or two radial elements are sufficient in many applications to represent the outgoing wave within the buffer zone, while for high-frequency excitations there is no need for a buffer zone. A graded mesh may be indicated in practice, especially if the excitation is broad-banded, or if it contains significant contributions from the higher angular modes.

2. Using  $\delta = \delta_{opt}$  improves significantly the performance of the viscoelastic boundary when it is placed near the region of physical interest; the improvement is greatest for the lower frequencies of excitation. This choice of  $\delta$  can be used to advantage in frequency-domain analyses and in time-domain calculations based on the FFT. It would, however, not be as practical for direct calculations in the time domain, since its frequency dependence would introduce convolutions into the corresponding expression [(11c)] for the boundary condition.

3. While all the calculations in this paper have been limited to the wave equation and a circular absorbing boundary, essentially the same method can be used to deal with more complex geometries, inhomogeneous materials, and scattering problems due to incident waves.

**ACKNOWLEDGMENT**

We thank Swanson Analysis Systems, Inc. for the support of the first writer through a Swanson Analysis Systems graduate fellowship in civil engineering. The work of the third writer was supported by the National Science Foundation under Grant DMS86-01288. We also thank the reviewers for their useful comments.

**APPENDIX I. ANALYTIC SOLUTIONS**

The amplitude  $U(r)$  of the response in (27) depends on the absorbing condition considered [one of (11a), (11b), or (11c)]. It can be expressed as:

$$U_{app} = \frac{\tau_0 r_1}{\mu} \frac{B_2 H_n^{(1)}(kr) - B_1 H_n^{(2)}(kr)}{A_1 B_2 - A_2 B_1} \dots \dots \dots (32)$$

in which

$$A_\alpha = nH_n^{(\alpha)}(kr_1) - kr_1 H_{n+1}^{(\alpha)}(kr_1) \dots \dots \dots (33a)$$

For (8a)

$$B_\alpha = \frac{1}{r_2} [nH_n^{(\alpha)}(kr_2) - kr_2 H_{n+1}^{(\alpha)}(kr_2)] + ikH_n^{(\alpha)}(kr_2) \dots \dots \dots (33b)$$

For (8b)

$$B_\alpha = \frac{1}{r_2} [nH_n^{(\alpha)}(kr_2) - kr_2 H_{n+1}^{(\alpha)}(kr_2)] + \left( \frac{1}{2r_2} + ik \right) H_n^{(\alpha)}(kr_2) \dots \dots \dots (33c)$$

For (8c)

$$B_\alpha = \frac{\delta + ik\beta}{r_2} [nH_n^{(\alpha)}(kr_2) - kr_2 H_{n+1}^{(\alpha)}(kr_2) - \left[ k^2\beta - ik\left(\frac{\beta}{2r_2} + \delta\right) - \frac{n^2\beta}{2r_2^2} + \left(\frac{\beta}{8r_2^2} - \frac{\delta}{2r_2}\right) \right] H_n^{(\alpha)}(kr_2) \dots \dots \dots (33d)$$

where  $\alpha = 1, 2$ . Similarly, the amplitude of the solution to the exact problem [(1a)-(1c)] can be written as:

$$U_{ex} = \frac{\tau_0 r_1}{\mu} \frac{H_n^{(2)}(kr)}{A_2} \dots \dots \dots (34)$$

In these equations,  $H_n^{(\alpha)}(\cdot)$  is the Hankel function of the  $\alpha$ th kind and order  $n$ .

**APPENDIX II. REFERENCES**

Barry, A., Bielak, J., and MacCamy, R. C. (1988). "On absorbing boundary conditions for wave propagation." *J. Comp. Phys.*, 79(2), 449-468.

Bayliss, A., and Turkel, E. (1980). "Radiation boundary conditions for wave-like equations." *Comm. Pure Appl. Math.*, 33(6), 707-725.

Blaschak, J. G., and Kriegsmann, G. A. (1988). "A comparative study of absorbing boundary conditions." *J. Comp. Phys.*, 77(1), 109-139.

Cohen, M., and Jennings, P. C. (1983). "Silent boundary methods for transient analysis." *Computational methods for transient analysis*, T. Belytschko and T. J. R. Hughes, eds., Elsevier Science Publishing Corp., New York, N.Y., 301-360.

Engquist, B., and Majda, A. (1977). "Absorbing boundary conditions for numerical simulation of waves." *Math. Comp.*, 31(139), 629-651.

Engquist, B., and Majda, A. (1979). "Radiation boundary conditions for acoustic and elastic wave calculations." *Comm. Pure Appl. Math.*, 32(3), 313-357.

Geers, T. L., and Felippa, A. C. (1983). "Doubly asymptotic approximations for vibration analysis of submerged structures." *J. Acoust. Soc. Am.*, 73(4), 1152-1159.

Halpern, L., and Trefethen, L. (1988). "Wide-angle one-way wave equations." *J. Acoust. Soc. Am.*, 84(4), 1397-1404.

Kallivokas, L. F. (1990). "Absorbing boundary conditions for wave propagation problems," thesis presented to Carnegie Mellon University, at Pittsburgh, Pa., in partial fulfillment of the requirements for the degree of Master of Science.

Kausel, E. (1988). "Local transmitting boundaries." *J. Engrg. Mech.*, 114(6), 1011-1027.

Kausel, E., and Tassoulas, J. L. (1981). "Transmitting boundaries: A closed-form comparison." *Bull. Seism. Soc. Am.*, 71(1), 143-159.

Kerr, A. D. (1964). "Elastic and viscoelastic foundation models." *J. Appl. Mech.*, 31, Sep., 491-498.

Kriegsmann, G. A., and Morawetz, C. S. (1978). "Numerical solutions of exterior problems with the reduced wave equation." *J. Comp. Phys.*, 28(2), 181-197.

Kriegsmann, G. A., Taflove, A., and Umashankar, K. R. (1987). "A new formulation of electromagnetic wave scattering using an on-surface radiation boundary condition approach." *IEEE Trans. Antennas Propag.*, AP-35(2), 153-160.

Lysmer, J., and Kuhlemeyer, R. (1969). "Finite dynamic model for infinite media." *J. Engrg. Mech.*, 95, 859-877.

Robinson, A. R. (1977). "The transmitting boundary-again." *Structural and geotechnical mechanics: A volume honoring Professor Nathan M. Newmark*, W. J. Hall, ed., Prentice-Hall, Englewood Cliffs, N.J.

Whitham, G. B. (1974). *Linear and nonlinear waves*. John Wiley and Sons, Inc., New York, N.Y.

Wolf, J. P. (1986). "A comparison of time-domain transmitting boundaries." *Earthq. Engrg. Struct. Dyn.*, 14(4), 655-673.

Downloaded from ascelibrary.org by University of Texas at Austin on 02/15/17. Copyright ASCE. For personal use only; all rights reserved.

### APPENDIX III. NOTATION

The following symbols are used in this paper:

$c_0, c_1, c_2$	=	coefficients of viscous damping [(20a) and (20b)];
$E(r)$	=	relative error [(30)];
$E, F, G$	=	boundary submatrices [(16b)];
$\mathcal{F}$	=	absorbing function operator [(4)];
$H(t)$	=	Heaviside function;
$H_n^{(1,2)}$	=	Hankel functions of first and second kind and of $n$ th order;
$i$	=	$\sqrt{-1}$ ;
$\mathbf{K}$	=	stiffness matrix [(16a)];
$\mathbf{k}$	=	boundary stiffness matrix [(25)];
$k$	=	wave number;
$k_0, k_1, k_2, k_3$	=	stiffness coefficients [(20a) and (20b)];
$\mathbf{M}$	=	mass matrix [(16a)];
$\mathbf{m}_1, \mathbf{m}_2$	=	boundary matrices [(25)];
$n$	=	angular mode of applied load [(26)];
$p$	=	dimensionless prescribed load [(1b)];
$\mathbf{p}$	=	load vector [(16b)];
$(r, \theta)$	=	polar coordinates;
$r_1, r_2$	=	radii of $\Gamma$ and $\Gamma_1$ , respectively;
$s$	=	Laplace transform variable;
$\mathbf{T}$	=	vector of nodal boundary tractions [(25)];
$t$	=	time;
$t_0$	=	reference time [(28)];
$U, U_{ex}, U_{app}$	=	displacement amplitudes;
$U_0$	=	reference displacement [(28)];
$u$	=	displacement, field variable;
$u_1, u_2, u_3$	=	displacements on viscoelastic boundary [(19a) and (19b)];
$\mathbf{u}_1, \mathbf{u}_2$	=	vectors of nodal boundary displacements [(21)];
$\mathbf{w}_3$	=	vector of nodal boundary slope [(22)];
$\beta$	=	velocity of SH waves;
$\Gamma$	=	inner boundary;
$\Gamma_1$	=	absorbing boundary;
$\gamma$	=	proportionality coefficient [(20b)];
$\Delta t$	=	time step;
$\delta, \delta_{cr}, \delta_{opt}$	=	stabilizing parameters;
$\zeta, \sigma, \phi, \psi$	=	vectors of shape functions;
$\eta$	=	wavelength;
$\kappa$	=	curvature;
$\lambda$	=	arc length;
$\mu$	=	shear modulus;
$\nu$	=	outward normal;
$\rho$	=	mass density;
$\tau, \tau_1, \tau_2$	=	tractions;
$\tau_0$	=	reference traction [(28)];
$v, v_1, v_2, v_3, \chi$	=	test functions;
$\Phi_m$	=	differential operators [(8) and (9)];
$\Omega, \Omega_1, \Omega_2, \Omega_3$	=	two-dimensional regions; and
$\omega$	=	angular frequency.